Avrupa Bilim ve Teknoloji Dergisi
Sayı 41, S. 393-399, Kasım 2022

Araştırma Makalesi

www.ejosat.com ISSN:2148-2683

European Journal of Science and Technology
No. 41, pp. 393-399, November 2022

Research Article

Liquid Sensor Based on Interaction between Decoupled Waveguides and a Cavity with Transverse Offset in a Phononic Crystal

Nurettin Korozlu[1*], Mehmet Günay[1], Ahmet Biçer[2], Ahmet Cicek[1]

[1*]Burdur Mehmet Akif Ersoy University, Faculty of Arts and Science, Department of Nanoscience and Nanotechnology, Burdur, Turkey,
(ORCID: 0000-0002-0899-0227), nkorozlu@mehmetakif.edu.tr
(ORCID: 0000-0001-8820-3520), mgunay@mehmetakif.edu.tr
(ORCID: 0000-0002-7686-0045), ahmetcicek@mehmetakif.edu.tr
[2]Burdur Mehmet Akif Ersoy University, Gölhisar Vocational School of Health Services, Department of Opticianry, Burdur, Turkey,
(ORCID: 0000-0002-7743-6078), ahmetbicer@mehmetakif.edu.tr

(İlk Geliş Tarihi 3 October 2022 ve Kabul Tarihi 9 November 2022)

(**DOI:** 10.31590/ejosat.1183694)

ATIF/REFERENCE: Korozlu, N., Günay, M., Biçer, A. & Cicek, A. (2022). Liquid Sensor Based on Interaction between Decoupled Waveguides and a Cavity with Transverse Offset in a Phononic Crystal. *Avrupa Bilim ve Teknoloji Dergisi*, (41), 393-399.

Abstract

A liquid sensor employing a cavity in the form of a point defect with a transverse offset along the normal bisector of a barrier at the center of a linear waveguide in a two-dimensional phononic crystal, which gives rise to two decoupled waveguides, is proposed. The phononic crystal consists of cylindrical steel rods with 2.0 mm radius in water, arranged with 4.2 mm lattice constant in the square lattice. Linear waveguides are formed by removing a single row from the phononic crystal, whereas the point defect is formed by substituting a single cylindrical steel rod by a polyethylene tubing comprising the analyte of interest. The cavity acts as a cross-bridge between the waveguides through the interaction of the linear defect mode in the input waveguide with the point defect mode, which in turn interacts with the output waveguide mode. Finite-element method simulations reveal that at frequencies around 200 kHz, a sharp peak with a quality factor of the order of 1000 occurs in the transmission spectrum of the system, where resonant transmission occurs. In case of determining the ratio of methanol in ethanol as an instance, it is found that the peak frequency exhibits a quadratic shift with the molar ratio of methanol. On the other hand, the transmission value decreases exponentially with increasing methanol ratio at the frequency of 196.19 kHz, which is the peak frequency for pure ethanol. The proposed sensing scheme can be utilized in many applications such as the identification of fake beverages and in high-throughput concentration measurements in the industry.

Keywords: Phononic crystal, Waveguide, Point defect, Liquid sensor, Ethanol, Methanol, Finite element method.

Bir Fononik Kristalde Ayrışmış Dalga Kılavuzları ile Dikine Ofsetli Kavite Arasında Eşleşmeye Dayalı Sıvı Sensörü

Öz

İki boyutlu bir fononik kristaldeki doğrusal dalga kılavuzunun merkezinde iki adet ayrışmış dalga kılavuzu oluşumuna sebep olan bariyerin dik ortayı üzerinde konumlanmış nokta kusuru formundaki bir kovuk içeren sıvı sensörü önerilmiştir. Fononik kristal, su içerisinde örgü sabiti 4.2 mm olacak biçimde kare örgü düzeninde dizilmiş 2.0 mm yarıçaplı silindirik çelik çubuklardan oluşmaktadır. Doğrusal dalga kılavuzları fononik kristalden tek bir sıranın çıkarılmasıyla oluşturulurken nokta kusuru, tek bir silindirik çelik çubuğun ilgili analiti içeren bir polietilen hortum ile değiştirilmesiyle oluşturulmuştur. Giriş dalga kılavuzundaki doğrusal kusur modunun daha sonra çıkış dalga kılavuzu moduyla etkileşen nokta kusur moduyla etkileşimi vasıtasıyla kovuk, iki dalga kılavuzu arasında çapraz bir köprü görevi görmektedir. Sonlu elemanlar yöntemi simülasyonlarının sonuçları, 200 kHz civarındaki frekanslarda

* Corresponding Author: nkorozlu@mehmetakif.edu.tr

sistemin geçirim spektrumunda 1000 mertebesinde kalite faktörüne sahip keskin bir pikin gözlendiği rezonans iletiminin oluştuğunu göstermiştir. Örnek olarak etanol içinde metanol oranı belirlenmesinde, pik frekansının molar metanol oranının karesiyle değiştiği belirlenmiştir. Öte yandan, saf etanol için belirlenen 196.19 kHz pik frekansında, geçirim değeri artan metanol oranıyla üstel olarak azalmaktadır. Önerilen algılama yaklaşımı, sahte içeceklerin tanımlanması ve endüstride yüksek verimli konsantrasyon ölçümleri gibi pek çok uygulamada kullanılabilir.

Anahtar Kelimeler: Fononik kristal, Dalga kılavuzu, Nokta kusuru, Sıvı sensörü, Etanol, Metanol, Sonlu elemanlar yöntemi.

1. Introduction

Non-invasive acoustic measurement methods, such as time-of-flight (Kuo et al., 1990), pulse-echo (Bamberger & Greenwood, 2004), and Doppler-shift measurements (Larrarte et al., 2008) are widely employed to determine particular physical properties, such as density, flow speed, and speed of sound, as well as the chemical composition of fluids. In the last decade, acoustic sensors involving artificial periodic structures called phononic crystals (PnCs) have been drawing intense attention to determine concentrations of binary liquid mixtures (Lucklum et al., 2010). The most prominent feature of PnCs is the existence of a band gap, i.e., a range of frequencies for which acoustic waves cannot propagate in the PnC (Kushwaha et al., 1993). One-dimensional (1D) and two-dimensional (2D) PnCs are commonly employed in sensing applications. A 1D PnC is obtained by periodic alternating stacking of layers with different acoustic properties. When a defect is formed by varying a single layer, the introduced cavity in the 1D PnC can be used in liquid concentration sensing (Aly & Mehaney, 2017; Lucklum & Li, 2009; Lucklum & Mukhin, 2021; Mehaney, 2019; Mehaney & Ahmed, 2020; Villa-Arango et al., 2017; Zaki et al., 2021).

2D PnCs are also widely employed in liquid sensing. For instance, extraordinary acoustic transmission across an array of periodic holes on a metal plate is employed to determine the molar ratio of 1-propanol in water (Ke et al., 2011). In addition, a 2D PnC with a cavity laid normally to the wave direction is employed (Lucklum et al., 2012; Oseev et al., 2013; Zubtsov et al., 2012). Interferometric sensors based on Mach-Zehnder interferometers implemented through waveguides (WGs) (Salman et al., 2021; Salman et al., 2014) or self-collimated waves (Salman et al., 2015) in 2D PnCs are also proposed. Recently, a compact sensor to determine the concentration of methanol in ethanol based on an add-drop filter in a 2D PnC is also proposed (Biçer et al., 2022).

A cavity in a 2D PnC is formed as a point defect where either a single scatterer is removed, or constituents of a single cell are modified. Such a cavity is associated with a sharp resonance peak with high quality factor in the band gap (Wu et al., 2001). PnC sensors based on cavity modes have been recently drawing attention as such sensors have small form factors and require small amount of analyte (Moradi et al., 2021; Mukhin et al., 2022; Zaremanesh et al., 2021). Due to the high quality factor, cavity-based sensors in 2D PnCs can offer high sensitivity, which is beneficial especially in determining the concentration in mixtures where the acoustical properties of the constituents are very similar. Thus, proposing new alternative and efficient cavity-based liquid sensors is important.

In this work, we propose a liquid concentration sensor based on the coupling of WG and point defect modes in a 2D PnC. Sensor design is such that a point defect comprising the analyte of interest, which is ethanol-methanol mixture in the present work, can act as a bridge between two decoupled WGs (DWGs), in a manner depending on the analyte concentration. It is numerically shown that the resonant transmission peak in the proposed sensor has a high quality factor and its frequency depends on the molar fraction of methanol in the mixture. In addition, sensing based on tracking acoustic pressure at a fixed frequency, where the output pressure decays rapidly with increasing methanol concentration, is also demonstrated.

2. Material and Method

The cavity-based liquid concentration sensor is depicted in Figure 1(a). Its backbone is a 2D PnC composed of a square array of steel cylinders in water background. The lattice constant and steel rod radii are set to a=4.2 mm and R=2.0 mm, respectively, corresponding to a filling ratio of 71.2%. Such a PnC has a broad band gap extending from 117.7 kHz to 265.7 kHz with a 77.1% gap-to-midgap ratio (Biçer et al., 2022; Salman et al., 2021). A linear defect WG to channelize acoustic waves in a range of frequencies (f) within the band gap is introduced by removing one row of steel rods from the PnC. Such a straight WG offers wave localization with a high transmission coefficient (Khelif et al., 2004).

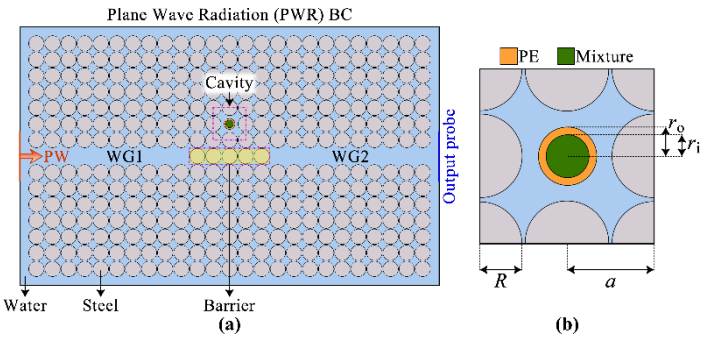

Figure 1: (a) Schematic view of the proposed cavity-based liquid concentration sensor and (b) a close-up view of the cavity.

The WG is split into two decoupled WGs by means of a barrier composed of N_x rows of steel rods. Figure 1(a) depicts the case for N_x=5. A resonant cavity aligned at the center of the barrier with a vertical separation index of N_y is introduced to facilitate wave transmission in a sharp resonance range. The cavity is composed of polyethylene (PE) tubing with inner and outer radii of r_i=1.0 mm and r_o=1.4 mm, respectively. The tubing is filled with ethanol-methanol binary mixture. The choice of PE as the tubing material stems from the fact that its acoustic impedance is comparable to that of water, thus preventing significant reflection losses (Biçer et al., 2022; Salman et al., 2021). Such a sensor design offers high sensitivity, where a small amount of analyte (mixture) is required, and sample reloading is practical. One can reload the sample compartment by injecting a new analyte along the tubing.

Finite-element method (FEM) simulations are carried out to calculate the eigenfrequencies to obtain the dispersion curves of the PnC, WG, and point defect, as well as to simulate the sensor operation as a function of the mixture concentration. The acoustic-structure model of the COMSOL Multiphysics software package (COMSOL, 2022) is utilized in FEM simulations. In this model, the acoustic and elastic wave equations are solved simultaneously with boundary conditions where the normal acceleration in the solid part of a boundary causes pressure variations in the fluid part, and pressure variations in the fluid give rise to normal forces on the solid part.

The fluid regions (i.e., water, ethanol, and ethanol-methanol mixture) are defined through the density (ρ) and speed of sound (c_s). The densities of water, ethanol, and methanol are taken as 999.6 kg/m^3 (COMSOL, 2022), 783.9 kg/m^3, and 786.5 kg/m^3 (Brown et al., 1988), at 293.15 K (20 °C), respectively, whereas the corresponding c_s are 1481.4 m/s (COMSOL, 2022), 1142.3 m/s, and 1103.0 m/s (Brown et al., 1988). This indicates that the density of pure methanol is only 0.3% different than the density of pure ethanol, while the discrepancy in the speed of sound is 3.4%. Detection of such small changes by acoustic means is relatively challenging. Variation of ρ and c_s with molar fraction of methanol in the ethanol-methanol mixture (R_m) is deduced from experimental data (Iglesias et al., 1998).

The solid components (steel and PE) in FEM simulations are defined through ρ, the Young's modulus (E), and the Poisson's ratio (ν). The densities are 7850 kg/m^3 and 930 kg/m^3 for steel and PE, respectively, whereas E=205 GPa and 1 GPa, and ν=0.28 and 0.40 (COMSOL, 2022).

Band structure of a straight WG is obtained in two stages. First, projection of the bands of the bulk PnC along the WG direction (i.e., the ΓX direction) is obtained. Then, the WG eigenfrequencies are calculated. In the latter, a supercell containing 11 rows and 1 column, where the central rod is removed, depicted in Figure 2(a) is employed. Parallel edges of the supercell are interrelated through Bloch-Floquet periodic boundary condition (PBC). Use of the PBC implies infinitely-long parallel WGs with 11a separation between adjacent WGs. The separation is adequately large so that neighboring virtual images of the WG interact negligibly with the WG, thus assuring well-converged dispersion curves. Eigenfrequencies for each wave vector (k_x, k_y=0) on the path $0 \le k_x \le \pi/a$ are obtained through the COMSOL software.

Projection of the bulk bands are obtained by considering the supercell in Figure 2(a), where the central rod is not removed. In this case, dispersion curves for a set of k_y values ranging between $-\pi/11a \le k_y \le \pi/11a$ are obtained. Here, a total of 21 k_y values are considered. Then, the plots are merged, and the projected bulk band ranges are obtained. Finally, the WG band structure is overlaid on the projected bulk bands to differentiate the modes arising from the linear defect.

Eigenfrequency analysis is also applied to an isolated cavity to obtain cavity resonances and to investigate how the resonance frequency (f_0), i.e., the cavity mode frequency within the linear defect band rage, varies with the molar methanol fraction (R_m) in the mixture. A square supercell containing 11 rows and 11 columns is employed in cavity eigenfrequency calculations.

FEM simulations for the computational model in Figure 2(a) is carried out by assuming time-harmonic acoustic waves, i.e., $p(x,y,t)=p(x,y)e^{-i2\pi ft}$, where p is the acoustic pressure. Thus, frequency-domain FEM simulations are carried out for a range of frequencies around f_0. The output spectra for different R_m are obtained and the results are analyzed to evaluate sensing performance. The input in Figure 2(a) is defined as a plane wave (PW) with 3a height at the center of the left edge of the domain. The output is probed at the right edge of the domain over a line of 3a height. Here, the pressure is calculated at the corresponding mesh nodes and its absolute value is averaged over the length of the probe line. As a result, the output average pressure (p_{avg}) is obtained. The computational domain in Figure 2(a) is terminated through a non-reflecting boundary condition, i.e., plane-wave radiation (PWR) BC through Givoli and Neta's reformulation of the Higdon conditions for plane waves to the second order (Givoli & Neta, 2003).

3. Results and Discussion

The WG band structure is presented in Figure 2(b). Here, the (green) shaded regions denote the projected bulk bands, corresponding to modes extending into the bulk of the PnC. Four bands appear within the PnC band gap range in Figure 2(b). The lowest-lying and highest-lying bands extend from the projected bulk bands and are associated with poor mode localization within the WG core. On the other hand, the two well-separated bands are candidates for wave channelization along the WG. However, the lower one of these comprises eigenmodes which are antisymmetric (odd) with respect to the horizontal bisector of the WG, and thus it is called a "deaf" band (Vasseur et al., 2005). A plane wave (PW) impinging on the WG cannot couple to these odd-parity modes. In contrast, the inset in Figure 2(b) shows that the eigenmodes of the linear defect (LD) band are symmetric (even). Thus, wave channelization is achieved through the modes on this band, which extends from 188 kHz to 238 kHz.

The transmission spectrum of the straight WG (solid black line) is given in Figure 2(c). Transmittance in the decibel (dB) scale is obtained through T (dB)=20x$\log_{10}(p_{avg}/p_{max})$, where p_{max} is the maximum p_{avg} value for the straight WG. The straight WG is associated with high transmission within its range, Figure 2(c). The spectrum exhibits Fabry-Perot oscillations due to finite WG length. Besides, transmission spectra for DWGs with different barrier thicknesses are also given in Figure 2(c). All spectra are calculated for 180 kHz$\le f \le$220 kHz with 10 Hz steps. It is seen that transmission at all frequencies drops significantly as N_x increases. T is always below -50 dB for N_x=5, indicating that the N_x=5 barrier is efficient in decoupling the WGs.

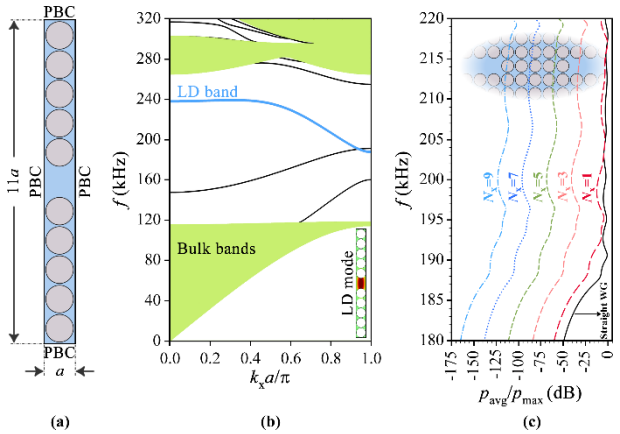

Figure 2: (a) Supercell geometry employed in straight WG band structure calculations, (b) the band structure of the WG, and (c) transmission spectra through the DWGs for different N_x. The case for N_x=5 is depicted in the background of (c).

When a plane wave with a frequency of f=196 kHz is incident from the left on a straight WG, whose width is 25a, it propagates in the linear defect in a well-localized manner and the transmission across the WG is high, Figure 3(a). However, the barrier in Figure 2(b) acts as a reflector for the same wave, as the frequency is within the PnC band gap. Thus, efficient WG decoupling, where transmission from the output WG is negligible, can be achieved with a N_x=5 barrier. The situation is different when a cavity is introduced, as will be shown later.

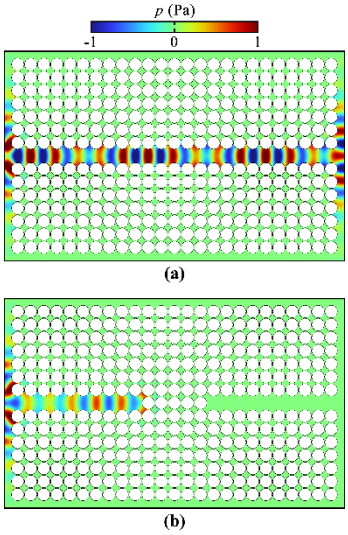

Figure 3: Propagation of an acoustic wave with f=196 kHz along a (a) straight WG and (b) decoupled WGs.

Cavity eigenfrequency calculations reveal that an isolated hollow-core cavity, which is a point defect where a single rod is removed, has a resonant mode which is even with respect to both x and y axes, as seen in the top panel of Figure 4(a). The point defect resonant mode frequency is calculated as f_0=211.06 kHz. Comparison of the top and bottom panels of Figure 4(a) reveals that the acoustic field profile is preserved even though a mixture-filled PE tubing is introduced. However, the mode frequency shifts to f_0=196.19 kHz. Similarly, the tubing displacement profile, shown in the close-up view in the bottom panel of Figure 4(a), is also even with respect to both axes.

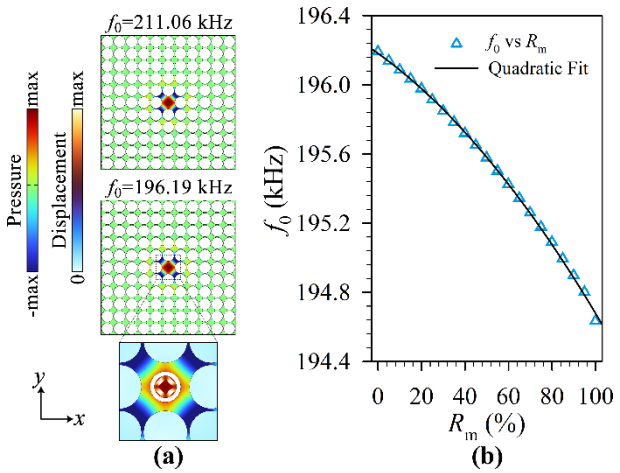

Figure 4: (a) Resonant mode shapes for a hollow-core (top) and analyte-filled PE tubing containing (bottom) cavity and (b) variation of the point defect resonant mode frequency as a function of the ratio of methanol in ethanol (R_m).

f_0 depends directly on R_m. Although c_s in the ethanol-methanol mixture decreases linearly with increasing R_m (Iglesias et al., 1998), Figure 4(b) shows that f_0 of the tubing-containing cavity exhibits a faster decrease rate. Thus, a quadratic fit with a coefficient of determination of R^2=0.998 represents the variation in Figure 4(b), well. This variation in f_0 results in the shift of the resonant transmission peak of the sensor system in Figure 1(a).

When the cavity is introduced above the center of the DWGs in Figure 3(b) at a distance of $N_y a$ so that the cavity-bridged system in Figure 1(a) is formed, the output p_{avg} becomes non-negligible for a narrow frequency range around f_0 of the isolated cavity with R_m=0%. As a result, a narrow symmetric transmission peak, as seen in Figure 5(a), is observed. For N_y=2, the transmission peak has a center frequency of f_p=196.19 kHz (which is equal to f_0 of the isolated cavity), and full width at half maximum (FWHM) of 22 Hz. This corresponds to a significantly high-quality factor of Q=8.9x10^3. Although symmetric, the transmission peak is not Gaussian. Instead, it has a Lorentzian line shape, as suggested by the Lorentzian fit with R^2=0.988 in Figure 5(a). This is due to homogeneous line shape broadening arising from cavity-WG interactions.

The resonant transmission peak shifts to lower frequencies (redshifts) with increasing R_m. The shift rate increases as R_m becomes closer to 100%, indicating a non-linear behavior. Besides, the peak shape is preserved for all R_m where the peak height varies between 1.6 Pa and 2.2 Pa in a smooth manner. However, no monotonic behavior is observed, i.e., the peak height rises to maximum for R_m around 80%, and then decreases. Besides, the peak FWHM decreases from 22 Hz to 14 Hz, as R_m increases from 0% to 100%.

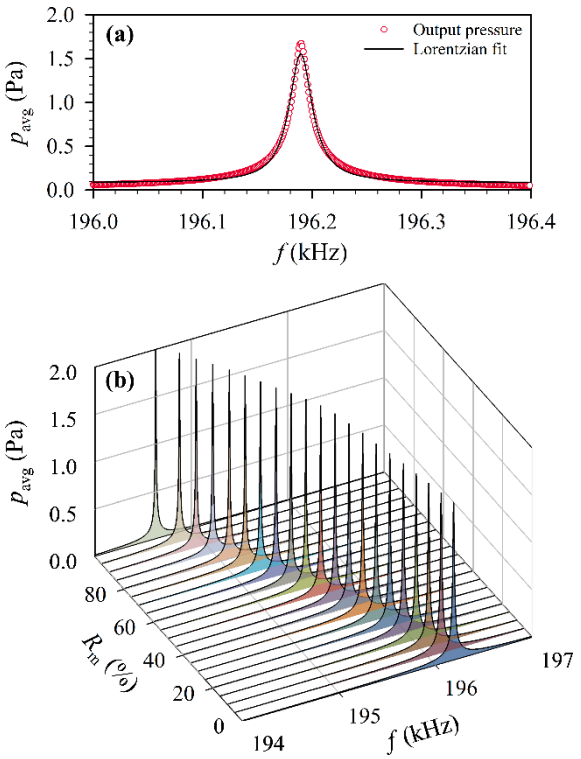

Figure 5: (a) Resonant transmission peak for N_x=5, N_y=2, and R_m=0% and (b) the peak behavior as a function of R_m.

The variation of resonant transmission peak frequency (Δf_p) with R_m is presented in Figure 6(a). The monotonic decrease is not linear, but quadratic, as evidenced by the linear (dashed line) and quadratic (solid line) fit curves in Figure 6(a). Thus, Δf_p in Figure 6(a) exhibits a parallel behavior to f_0 in Figure 4(b). On the other hand, the shift rate is slower for $R_m \leq 20\%$. The inset in Figure 6(a) for Δf_p data calculated in this range with 1% R_m steps demonstrates a linear variation. The slope of the linear fit (dashed line) in the inset of Figure 6(a) is -10.63 Hz/% molar fraction of methanol. Although a single sample cell (mixture-filled PE tubing) is involved, such a sensitivity is comparable to that obtained through an add-drop filter (i.e., 12.4 Hz/%) (Biçer et al., 2022) and higher than the one obtained through a Mach-Zehnder interferometer (i.e., 6.20 Hz/%) (Salman et al., 2021).

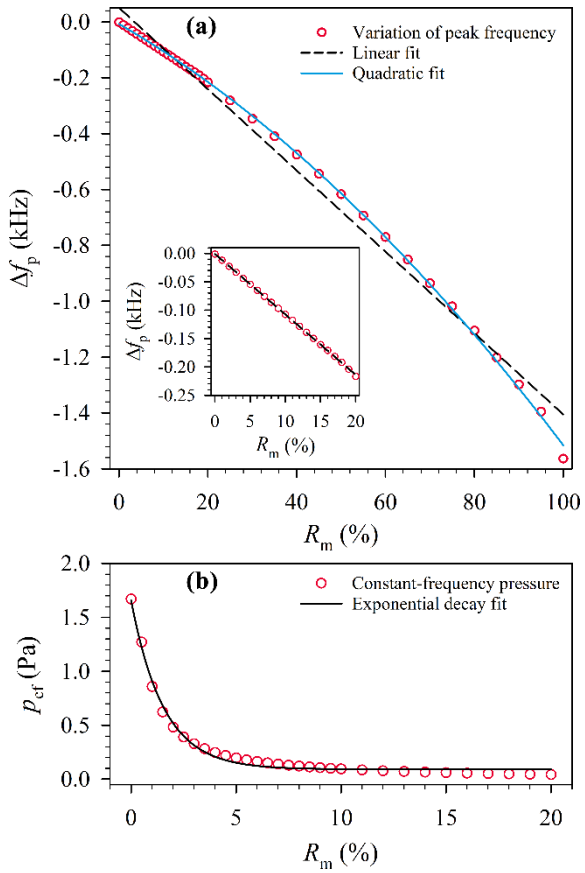

Figure 6: (a) The frequency shift of the resonant transmission peak and (b) variation of the output pressure at f_p=196.19 kHz as a function of R_m. The inset in (a) is a close-up view of the frequency shift for $R_m \leq 20\%$.

As the resonant peak redshifts linearly for $R_m \leq 20\%$, the p_{avg} value at f_p=196.19 kHz is expected to drop rapidly with increasing R_m. Thus, even a small change in R_m can cause a large drop in the measured output pressure at constant frequency (p_{cf}, i.e., p_{avg} at 196.19 kHz). Figure 6(b) shows that p_{cf} exhibits a sharp decaying behavior with R_m. The exponential fit in Figure 6(b) in the form of $p_{cf}(R_m) = p_0 + A \cdot e^{-\alpha R_m}$ reveals that the decay rate is α=0.648 per percent variation of R_m, where p_0=0.097 Pa and A=1.564 Pa. The fact that $p_0 \neq 0$ stems from the fact that the Lorentzian line shape in Figure 5(a) has a long tail. Thus, small methanol concentrations can be detected with high sensitivity by tracking the p_{cf}.

The resonant transmission peak for N_y=3 is given in Figure 7(a). It is a sharper peak than in Figure 5(a) for N_y=2, as cavity-WG interactions become weaker with increasing N_y. Its central frequency is f_p=196.19 kHz, as in the case for N_y=2, and FWHM is approximately 0.6 Hz with a much higher Q factor of 3.3x10^5.

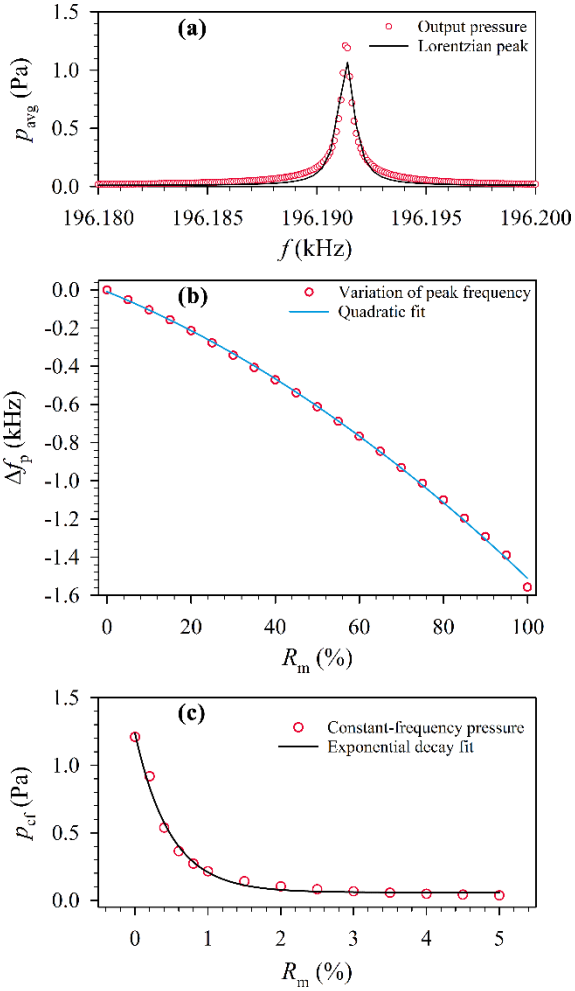

Figure 7: (a) A zoomed view of the resonant transmission peak for N_x=5, N_y=3, and R_m=0%, as well as dependence of (b) the associated frequency shift and (c) variation of the output pressure at f_p=196.19 kHz on R_m.

Variation of f_p with R_m is depicted in Figure 7(b). Again, a quadratic variation is observed for N_y=3. Comparison of Figure 6(a) and Figure 7(b) reveals that N_y=2 and N_y=3 cavities have very similar $\Delta f_p(R_m)$ behavior. Thus, either one can be used for sensing purposes. In contrast, comparison of Figure 6(b) and Figure 7(c) reveals that the decay rate is faster for N_y=3. The exponential decay fit parameters are found out to be p_0=0.062 Pa, A=1.176 Pa, and α=2.062 per percent variation of R_m. Thus, N_y=3 cavity offers higher sensitivity in terms of p_{cf} for $R_m \leq 5\%$.

4. Conclusions and Recommendations

A liquid concentration sensor based on tunable coupling between a point defect and two decoupled waveguides in a two-dimensional phononic crystal is demonstrated. As the liquid-solid phononic crystal has a broad acoustic band gap, the linear defect waveguide possesses guiding modes over a relatively broad range from 188 kHz to 238 kHz. However, the waveguide is split into two decoupled waveguides by introducing a barrier layer at the center. It is seen that a barrier with 5 columns of scatterers can adequately decouple the split waveguides. An isolated point defect where a single scatterer is removed has a resonant mode at approximately 211 kHz, whereas the resonant frequency is around 196 kHz when the cavity is formed by a polyethylene tubing filled with ethanol-methanol mixture. The cavity acts as a bridge between the decoupled waveguides and facilitates resonant tunneling when it is introduced above the barrier with a transverse offset.

The resonant transmission frequency varies as a function of the molar methanol concentration, where the shift rate is quadratic. However, an almost linear operation is observed when the methanol concentration is below 20%. As a result, a sensitivity of 10.63 Hz per percent variation of methanol concentration is obtained in this range. In addition, the measured output frequency decreases exponentially with increasing methanol concentration. Moreover, the decay rate is higher for a farther cavity. Thus, the proposed sensor can be employed in detecting small concentrations with high sensitivity.

The proposed liquid concentration sensor has a small footprint where the phononic crystal covers 15x25 periods (i.e., 8.2-by-13.2 wavelengths at 196 kHz). Moreover, the required analyte volume is very small. Assuming that the phononic crystal height is 25 mm (approximately 5.9 periods), the inner tubing volume is 19.6 mm^3, and thus only approximately 20 μL of ethanol-methanol mixture is required (neglecting dead volume in the connection tubing) for sensing. Furthermore, sample changing is practical: first flush out the previous sample, then wash by pure ethanol and dry, and finally inject a new sample. Influence of temperature variations can be ruled out by monitoring and controlling the temperature through a thermocouple and Peltier cell, respectively. Input and output can be provided by a couple of ultrasonic transducers with resonance frequencies around 200 kHz. The control electronics would be simple, as continuous sine wave is required as a source. Finally, the sensor can be calibrated for other binary liquid mixtures. In brief, a practical acoustic liquid concentration sensor which can be realized at low cost is proposed and numerically investigated.

5. Acknowledgement

This work is supported by the Scientific and Technological Research Council of Turkey (TÜBİTAK) under grant number: 116F085. Ahmet Cicek acknowledges support from Turkish Academy of Sciences (TÜBA) Outstanding Young Researchers Awarding Programme (GEBİP-2018).

References

Aly, A. H., & Mehaney, A. (2017). Phononic crystals with one-dimensional defect as sensor materials. *Indian Journal of Physics*, *91*(9), 1021-1028. https://doi.org/https://doi.org/10.1007/s12648-017-0989-z

Bamberger, J. A., & Greenwood, M. S. (2004). Measuring fluid and slurry density and solids concentration non-invasively. *Ultrasonics*, *42*(1-9), 563-567. https://doi.org/https://doi.org/10.1016/j.ultras.2004.01.032

Biçer, A., Durmuslar, A. S., Korozlu, N., & Cicek, A. (2022). An Acoustic Add-Drop Filter in a Phononic Crystal for High-Sensitivity Detection of Methanol in Ethanol in the Liquid Phase. *IEEE Sensors Journal*, *22*(15), 14799-14805. https://doi.org/10.1109/JSEN.2022.3185926

Brown, J., Slutsky, L., Nelson, K., & Cheng, L.-T. (1988). Velocity of sound and equations of state for methanol and ethanol in a diamond-anvil cell. *Science*, *241*(4861), 65-67. https://doi.org/https://doi.org/10.1126/science.241.4861.65

COMSOL, Inc. (2022). *COMSOL-Software for Multiphysics Simulation*. Retrieved 30.09.2022 from https://www.comsol.com

Givoli, D., & Neta, B. (2003). High-order non-reflecting boundary scheme for time-dependent waves. *Journal of Computational Physics*, *186*(1), 24-46. https://doi.org/10. 1016/S0021-9991(03)00005-6

Iglesias, M., Orge, B., Domínguez, M., & Tojo, J. (1998). Mixing properties of the binary mixtures of acetone, methanol, ethanol, and 2-butanone at 298.15 K. *Physics and Chemistry of Liquids*, *37*(1), 9-29. https://doi.org/10.1080/00319109808032796

Ke, M., Zubtsov, M., & Lucklum, R. (2011). Sub-wavelength phononic crystal liquid sensor. *Journal of Applied Physics*, *110*(2), 026101. https://doi.org/10.1063/1.3610391

Khelif, A., Choujaa, A., Benchabane, S., Djafari-Rouhani, B., & Laude, V. (2004). Guiding and bending of acoustic waves in highly confined phononic crystal waveguides. *Applied Physics Letters*, *84*(22), 4400-4402. https://doi.org/10.1063/1.1757642

Kuo, I., Hete, B., & Shung, K. (1990). A novel method for the measurement of acoustic speed. *The Journal of the Acoustical Society of America*, *88*(4), 1679-1682. https://doi.org/10.1063/1.400242

Kushwaha, M. S., Halevi, P., Dobrzynski, L., & Djafari-Rouhani, B. (1993). Acoustic band structure of periodic elastic composites. *Physical Review Letters*, *71*(13), 2022. https://doi.org/10.1103/PhysRevLett.71.2022

Larrarte, F., Bardiaux, J. B., Battaglia, P., & Joannis, C. (2008). Acoustic Doppler flow-meters: a proposal to characterize their technical parameters. *Flow Measurement and Instrumentation*, *19*(5), 261-267. https://doi.org/10.1016/j.flowmeasinst.2008.01.001

Lucklum, R., Ke, M., & Zubtsov, M. (2012). Two-dimensional phononic crystal sensor based on a cavity mode. *Sensors and Actuators B: Chemical*, *171*, 271-277. https://doi.org/10.1016/j.snb.2012.03.063

Lucklum, R., & Li, J. (2009). Phononic crystals for liquid sensor applications. *Measurement Science and Technology*, *20*(12), 124014. https://doi.org/10.1088/0957-0233/20/12/124014

Lucklum, R., Li, J., & Zubtsov, M. (2010). 1D and 2D phononic crystal sensors. *Procedia Engineering*, *5*, 436-439. https://doi.org/10.1016/j.proeng.2010.09.140

Lucklum, R., & Mukhin, N. (2021). Enhanced sensitivity of resonant liquid sensors by phononic crystals. *Journal of Applied Physics*, *130*(2), 024508. https://doi.org/10.1063/5.0046847

Mehaney, A. (2019). Biodiesel physical properties detection using one-dimensional phononic crystal sensor. *Acoustical Physics*, *65*(4), 374-378. https://doi.org/10.1134/S1063771019040122

Mehaney, A., & Ahmed, A. M. (2020). Theoretical design of porous phononic crystal sensor for detecting CO_2 pollutions in air. *Physica E: Low-Dimensional Systems and Nanostructures*, *124*, 114353. https://doi.org/10.1016/j.physe.2020.114353

Moradi, P., Gharibi, H., Fard, A. M., & Mehaney, A. (2021). Four-channel ultrasonic demultiplexer based on two-dimensional phononic crystal towards high efficient liquid sensor. *Physica Scripta*, *96*(12), 125713. https://doi.org/10.1088/1402-4896/ac2c23

Mukhin, N., Kutia, M., Aman, A., Steinmann, U., & Lucklum, R. (2022). Two-Dimensional Phononic Crystal Based Sensor for Characterization of Mixtures and Heterogeneous Liquids. *Sensors*, *22*(7), 2816. https://doi.org/10.3390/s22072816

Oseev, A., Zubtsov, M., & Lucklum, R. (2013). Gasoline properties determination with phononic crystal cavity sensor. *Sensors and Actuators B: Chemical*, *189*, 208-212. https://doi.org/10.1016/j.snb.2013.03.072

Salman, A., Ates, E., Biçer, A., Deniz, S., Cicek, A., & Korozlu, N. (2021). Determination of Methanol Concentration in Ethanol in Liquid Phase by a Phononic Crystal Mach-Zehnder Interferometer. *Physica Scripta, 96(12)*, 125032. https://doi.org/10.1088/1402-4896/ac3d4b

Salman, A., Kaya, O. A., & Cicek, A. (2014). Determination of concentration of ethanol in water by a linear waveguide in a 2-dimensional phononic crystal slab. *Sensors and Actuators A: Physical*, *208*, 50-55. https://doi.org/10.1016/j.sna.2013.12.037

Salman, A., Kaya, O. A., Cicek, A., & Ulug, B. (2015). Low-concentration liquid sensing by an acoustic Mach–Zehnder interferometer in a two-dimensional phononic crystal. *Journal of Physics D: Applied Physics*, *48*(25), 255301. https://doi.org/https://doi.org/10.1088/0022-3727/48/25/255301

Vasseur, J. O., Deymier, P. A., Beaugeois, M., Pennec, Y., Djafari-Rouhani, B., & Prevost, D. (2005). Experimental observation of resonant filtering in a two-dimensional phononic crystal waveguide. *Zeitschrift für Kristallographie-Crystalline Materials*, *220*(9-10), 829-835. https://doi.org/10.1524/zkri.2005.220.9-10.829

Villa-Arango, S., Torres, R., Kyriacou, P., & Lucklum, R. (2017). Fully-disposable multilayered phononic crystal liquid sensor with symmetry reduction and a resonant cavity. *Measurement*, *102*, 20-25. https://doi.org/10.1016/j.measurement.2017.01.051

Wu, F., Hou, Z., Liu, Z., & Liu, Y. (2001). Point defect states in two-dimensional phononic crystals. *Physics Letters A*, *292*(3), 198-202. https://doi.org/10.1016/S0375-9601(01)00800-3

Zaki, S. E., Mehaney, A., Hassanein, H. M., & Aly, A. H. (2021). High-performance liquid sensor based one-dimensional phononic crystal with demultiplexing capability. *Materials Today Communications*, *26*, 102045. https://doi.org/10.1016/j.mtcomm.2021.102045

Zaremanesh, M., Carpentier, L., Gharibi, H., Bahrami, A., Mehaney, A., Gueddida, A., Lucklum, R., Djafari-Rouhani, B., & Pennec, Y. (2021). Temperature biosensor based on triangular lattice phononic crystals. *APL Materials*, *9*(6), 061114. https://doi.org/10.1063/5.0054155

Zubtsov, M., Lucklum, R., Ke, M., Oseev, A., Grundmann, R., Henning, B., & Hempel, U. (2012). 2D phononic crystal sensor with normal incidence of sound. *Sensors and Actuators A: Physical*, *186*, 118-124. https://doi.org/10.1016/j.sna.2012.03.017